A 3D finite element static and free vibration analysis of magneto-electro-elastic beam

Vinyas. M and S. C. Kattimani[*]

Department of Mechanical Engineering, National Institute of Technology Karnataka, Surathkal-575025, India

Abstract. In this paper, free vibration and static response of magneto-electro-elastic (MEE) beams has been investigated. To this end, a 3D finite element formulation has been derived by minimization the total potential energy and linear constitutive equation. The coupling between elastic, electric and magnetic fields can have a significant influence on the stiffness and in turn on the static behaviour of MEE beam. Further, different Barium Titanate (BaTiO$_3$) and Cobalt Ferric oxide (CoFe$_2$O$_4$) volume fractions results in indifferent coupled response. Therefore, through the numerical examples the influence of volume fractions and boundary conditions on the natural frequencies of MEE beam is illustrated. The study is extended to evaluate the static response of MEE beam under various forms of mechanical loading. It is seen from the numerical evaluation that the volume fractions, loading and boundary conditions have a significant effect on the structural behaviour of MEE structures. The observations made here may serve as benchmark solutions in the optimum design of MEE structures.

Keywords: magneto-electro-elastic; volume fractions; piezoelectric and piezomagnetic, free vibration

1. Introduction

Smart materials are the trending materials which has grasped the attention of the entire research community in recent years. Due to their self-responding and self-adaptive capabilities, it has become a boon to the structural engineering. A special class of materials formed by combining the piezoelectric (BaTiO$_3$) and magnetostrictive (CoFe$_2$O$_4$) materials commonly known as MEE materials are the prominent material which exhibits a significant interaction between magnetic, elastic and electric and properties. The elastic deformations are induced directly by the application of the mechanical load and indirectly by the electric or magnetic fields. As a result, the electric polarization and magnetic polarization can be controlled through magnetic and electric fields, respectively. Further, in these materials conversion of energy from one form into another is highly feasible. Hence, the potentiality of these materials is exploited in various engineering applications such as aerospace industry, automobiles industry, sensors and actuators, etc.

Many pioneers have evaluated the different structural behavior such as free vibrations, static

---

*Corresponding author, E-mail: sck@nitk.ac.in

analysis and buckling analysis of the MEE structures. Few prominent literatures among them have been highlighted here. Milazzo (2013) investigated the dynamic problem of a MEE beam by employing first order shear deformation theory. Annigeri *et al*. (2007) evaluated the influence of coupling effects on the natural frequency of the multiphase MEE beams. Bhangale *et al*. (2006) investigated the free vibration analysis of MEE plates using semi-analytical FE method. Milazzo *et al*. (2009) performed free and forced vibration analysis of bimorph beams and proposed an analytical solution for both multiphase and laminated MEE beams. Huang *et al*. (2007) analytically computed the behavior of the functionally graded (FG) MEE beams subjected to an arbitrary loading. Pan *et al*. (2005) presented the exact solutions for the multilayered MEE plates subjected to internal and surface loading. Biju *et al*. (2011) used 3D magnetic vector potential approach to analyse the response of multiphase MEE sensors. They have also studied the effect of different volume fraction on the responses. Using meshless local integral equation Sladek *et al*. (2017) evaluated the effective material properties in MEE composite materials. Fan *et al*. (2016) analysed the laminated composites by making use of the C^0 type Reddy theory considering transverse normal thermal strain. Lage *et al*. (2004) carried out the static analysis of MEE structures using a layerwise partial mixed FE model. Chen *et al*. (2007) made use of state vector approach to carry out the modal analysis of the MEE plates. Kattimani and Ray (2014a, b, 2015) proposed a FE method to reduce the large amplitude vibrations of smart MEE plates and doubly curved shells through the active constrained layer damping (ACLD). They further extended their study to analyse the FG-MEE plates. Using higher order finite element model, static and free vibration analysis for MEE plates are carried out by Moita *et al*. (2009). The non-linear large deflections of the MEE plates subjected to mechanical and magneto-electric loads is evaluated using a meshless local Petrov*Galerkin method by Sladek *et al*. (2013). Carrera *et al*. (2009) developed a FE model based on the Reissner's Mixed Variational Theorem RMVT for the static analysis of the MEE plates subjected to different fields. Recently, Benedetti and Milazzo (2017) developed families of equivalent single layer and multilayered model for free and static analysis of MEE plates. Liu *et al*. (2016) obtained higher order solutions for MEE plate with non-uniform materials using scaled boundary FE method. Aktas (2001) derived the deformation function of the orthotropic beam using anisotropic elasticity. Balu *et al*. (2014) investigated the behavior of the MEE beam subjected to mechanical and thermal loadings. They also studied the effect of the layup sequences on the displacement and potentials. Arefi and Zenkour (2017) presented a governing equations for MEE curved beams based on first order shear deformation theory. Ebrahimi *et al*. (2017) studied the effect of porosity on the vibration characteristics of MEE plates. The geometrically nonlinear vibrations of multiferroic composite plate and shell was analysed by Kattimani (2017).

Analyzing the influence of nano and micro structures are crucial in numerous intelligent structures. Vaezi *et al*. (2016) studied the free vibration analysis of the MEE micro beams under magneto-electric loads. Simsek and Reddy (2013) presented a new size dependant unified beam theory to analyse the static and free vibration behavior of the FG micro beams. Ebrahimi and Barati (2016a) presented an analytical solution to assess the free vibration characteristics of magneto-electro-viscoelastic nano beams. In addition, Ebrahimi and Barati (2016b, c) studied the influence of different temperature loads on the free vibration behavior of FG-MEE nanobeams. Jandaghian and Rahmani (2016) evaluated the effect of elastic foundation on the free vibration of magneto-electro-thermo-elastic beams.

Few studies have been reported on thermal analysis of MEE structures. Kumaravel *et al.* (2007) studied the influence of both uniform and non-uniform load on the static behavior of MEE beam.

Kondaiah *et al*. (2012) studied the pyroeffects on the structural behaviour of MEE beam subjected to temperature loading. Further, Kondaiah *et al*. (2015, 2017) they extended their evaluation to analyze the pryroeffects on the MEE sensor patch. More recently, Vinyas and Kattimani (2017a, b and c) developed a FE formulation and analyzed the thermal response of MEE beam and plates. They extended their evaluation for multiphase MEE beams subjected to different temperature loading also (Vinyas and Kattimani 2017d). With the aid of 3D FE formulation, the influence of thermo-mechanical loads on the static response of MEE beam (Vinyas and Kattimani 2017e) and hygrothermal response of MEE plates has been thoroughly investigated (Vinyas and Kattimani 2017f).

Based on the comprehensive literature review, it is observed that the 3D finite element analysis of the free vibration and static behaviour of magneto-electro-elastic beams subjected to different forms of mechanical loads has not been reported. In this regard, this work makes a first attempt using 3D FE formulation. In addition, an effort is made to understand the influence of different boundary conditions and volume fractions on the natural frequency and static parameters of the MEE beam. The results presented here will serve as a benchmark solution in the design and analysis of MEE smart structures.

2. Governing equations

2.1 Linear coupled constitutive relationship

The linear relationship between the various fields of MEE materials can be explicitly represented as follows

$$\sigma_i = C_{ij}\varepsilon_j - e_{ik}E_k - q_{ik}H_k$$

$$D_l = e_{lj}\,\varepsilon_j + \eta_{lk}E_k + m_{lk}H_k B_l = q_{lj}\varepsilon_j + m_{lk}E_k + \mu_{lk}H_k \tag{1}$$

The different material properties in Eq. (1) are shown in Appendix A. Meanwhile, the strain field related to the displacements can be written as follows

$$\varepsilon_{ij} = \frac{1}{2}\left(u_{i,j} + u_{j.i}\right) \tag{2}$$

The relation between the electric field vector and the electric potential; magnetic field vector and magnetic potential can be represented as

$$E_i = -\phi_{,i}\,;H_i = -\psi_{,i} \tag{3}$$

The total potential π_p is given as follows

$$\pi_p = \frac{1}{2}\left(\int_\Omega \{\varepsilon\}^T \{\sigma\}\,d\Omega - \int_\Omega [E]^T \{D\}\,d\Omega - \int_\Omega [H]^T \{B\}\,d\Omega\right) - \int_A \{u\}^T \{F_{surface}\}\,dA$$

$$- \int_\Omega \{u\}^T \{F_{body}\}\,d\Omega - \{u\}^T \{F_{conc}\} - \int_A \phi\,Q^\phi\,dA - \int_A \psi\,Q^\psi\,dA \tag{4}$$

2.2 Finite element model

The degrees of freedom corresponding to each node are: displacement components (along *x, y* and *z* direction), electric potential and magnetic potential. Further, a 3D brick element is used for modeling the MEE beam. The nodal displacement, electric potential and magnetic potential can be expressed by suitable shape functions as follows

$$u = [N_u]\{u_i\}\,;\ \phi = [N_\phi]\{\phi\}\,;\ \psi = [N_\psi]\{\psi\} \tag{5}$$

where, $\{u_i\} = \{U_x, U_v, U_w\}$; N_u, N_ϕ, N_ψ are the shape functions. The following assumptions are made while deriving the deriving the FE formulation for the present case.
 • There exists a complete coupling between the magnetic, electric and elastic fields.
 • The effect of electric charge density and magnetic current densities are neglected.
 Finally, the coupled finite element equations obtained after simplification are written as

$$\left(\left[K_{uu}^e\right] - \omega^2\left[M^e\right]\right)\{u\} + \left[K_{u\phi}^e\right]\{\phi^e\} + \left[K_{u\psi}^e\right]\{\psi^e\} = \{F_m\}$$

$$\left[K_{u\phi}^e\right]^T\{u\} - \left[K_{\phi\phi}^e\right]\{\phi^e\} - \left[K_{\phi\psi}^e\right]\{\psi^e\} = 0 \tag{6}$$

$$\left[K_{u\psi}^e\right]^T\{u\} - \left[K_{\phi\psi}^e\right]^T\{\phi^e\} - \left[K_{\psi\psi}^e\right]\{\psi^e\} = 0$$

The different stiffness matrices in Eq. (6) and its corresponding expressions are presented in Appendix A and B, respectively. By eliminating the electric and magnetic potential through condensation technique, the equivalent stiffness matrix $[K_{eq}]$ is derived to obtain the nodal displacements.

$$[K_{eq}]\{u\} = \{F_{eq}\}$$

3. Results and discussion

3.1 Validation of finite element formulation

The results computed using present FE formulation are validated with the results reported by Balu *et al*. (2014). It should be noted that the FE formulation derived here can also be used for the pure elastic, pure piezoelectric and pure piezomagnetic beams by changing the properties and equating the irrelevant matrices to null matrices. Hence, in this case, the MEE beam is degenerated to the purely piezoelectric (BaTiO₃) beam. The beam geometry, material properties and loading conditions are considered as identical to that of Balu *et al*. (2014). Fig. 1 depicts the validation of the *z*-direction displacement component (U_w) of the pure piezoelectric cantilever beam subjected to the end load. It may be seen from this figure that the results from the present FE formulation are in excellent correlation with Balu *et al*. (2014). Further, using the uncoupled elastic formulation, the present code is used to validate the results of the composite beams subjected to a point load with different fiber orientation angles as presented by Aktas (2001). It may be noticed from Table 1 that the end deflections of the cantilever beam obtained from the present FE model accurately matches with the results reported by Aktas (2001) for different operating conditions and fiber orientation angles.
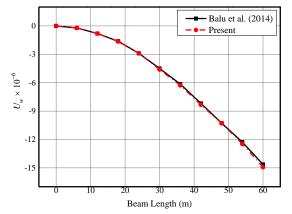
Fig. 1 Validation of the *z*-direction displacement component

Table 1 Validation of deflection of composite beams at free end

Fiber orientation			0	15	30	45	60	75	90
Deflection (mm)	Point load	Aktas (2001)	0.40	0.92	2.19	3.53	4.42	4.79	4.86
		Present	0.41	0.93	2.36	3.61	4.57	4.92	4.97
	UDL	Aktas (2001)	0.246	0.345	0.652	1.090	1.510	1.796	1.899
		Present	0.252	0.353	0.661	1.102	1.526	1.803	1.907

3.2 Structural analysis of the MEE beam

In this section, the free vibration and static analysis of the magneto-electro elastic (MEE) beams with different volume fraction (V_f) is analysed. The influence of different boundary conditions and various mechanical loadings on the static quantities has also been studied. A finite element (FE) model of the beam is developed using an eight noded 3D brick element. The material properties mentioned in Table 2 are used for the present analysis. The beam geometry has a length L=1 m, width w=0.3 m and thickness h=0.2 m.

3.3 Free vibration analysis

This section deals with evaluation of the influence of volume fraction on the natural frequencies of the MEE beam. The effect of boundary conditions on the natural frequencies has also been studied. Figs. 2 and 3 present the natural frequency variation for the first ten modes of the clamped-free and clamped-clamped MEE beam, respectively for the various volume fraction of the piezoelectric material. The same is also presented in Tables 3 and 4, respectively. It may be observed from these Figs. 2(a) and (b) and from the Tables 3 and 4 that the natural frequencies of the MEE beam decrease with the increase in the volume fraction. This may be due to the fact that as the volume fraction increases, the volume of the magnetostrictive material ($CoFe_2O_4$) increases which leads to increase in the value of the material constants. Influence of these material constants on the natural frequency may be observed clearly for the higher modes of vibration. It may also be noticed that the clamped-clamped boundary condition exhibits a higher value of natural frequency at each mode.
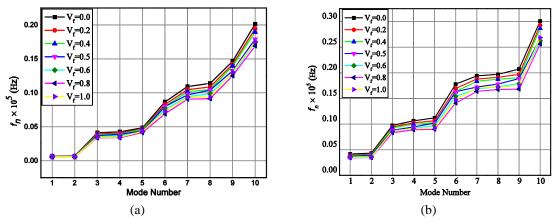
Fig. 2 Natural frequencies (a) clamped-free (b) clamped-clamped MEE beam

Table 2 Material co-efficients of BaTiO$_3$-CoFe$_2$O$_4$ composite w.r.t different volume fraction V$_f$ of BaTiO$_3$ (Kondaiah *et al.* 2012)

Material property	Material constants	0 V$_f$	0.2 V$_f$	0.4 V$_f$	0.5 V$_f$	0.6 V$_f$	0.8 V$_f$	1 V$_f$
Elastic constants (GPa)	$C_{11}=C_{22}$	286	250	225	220	200	175	166
	C_{12}	173	146	125	120	110	100	77
	$C_{13}=C_{23}$	170	145	125	120	110	100	78
	C_{33}	269.5	240	220	215	190	170	162
	$C_{44}=C_{55}$	45.3	45	45	45	45	50	43
	C_{66}	56.5	52	50	50	45	37.5	44.5
Piezoelectric constants (C/m^2)	e_{31}	0	-2	-3	-3.5	-3.5	-4	-4.4
	e_{33}	0	4	7	9.0	11	14	18.6
	e_{15}	0	0	0	0	0	0	11.6
Dielectric constant (10^{-9} C^2/Nm^2)	$\eta_{11}=\eta_{22}$	0.08	0.33	0.8	0.85	0.9	1	11.2
	η_{33}	0.093	2.5	5	6.3	7.5	10	12.6
Magnetic permeability (10^{-4} Ns^2/C^2)	$\mu_{11}=\mu_{22}$	-5.9	-3.9	-2.5	-2.0	-1.5	-0.8	0.05
	μ_{33}	1.57	1.33	1	0.9	0.75	0.5	0.1
Piezomagnetic constants (N/Am)	q_{31}	580	410	300	350	200	100	0
	q_{33}	700	550	380	320	260	120	0
	q_{15}	560	340	220	200	180	80	0
Magneto-electric constant (10^{-12}Ns/VC)	$m_{11}=m_{22}$	0	2.8	4.8	5.5	6	6.8	0
	m_{33}	0	2000	2750	2600	2500	1500	0
Pyroelectric-constant (10^{-7} C/m^{2}K)	p_2	0	-3.5	-6.5	-7.8	-9	-10.8	0
Pyromagnetic constant (10^{-5} C/m^{2}K)	τ_2	0	-36	-28	-23	-18	-8.5	0
Thermal expansion coefficient (10^{-6} K^{-1})	$\alpha_1=\alpha_2$	10	10.8	11.8	12.3	12.9	14.1	15.7
	α_3	10	9.3	8.6	8.2	7.8	7.2	6.4
Density (kg/m^3)	ρ	5300	5400	5500	5550	5600	5700	5800

Table 3 Natural frequencies for C-F MEE beam with different volume fractions

Mode No.	Natural Frequency (Hz)						
	$V_f = 0.0$	$V_f = 0.2$	$V_f = 0.4$	$V_f = 0.5$	$V_f = 0.6$	$V_f = 0.8$	$V_f = 1.0$
1	690	660	630	628	590	560	558
2	700	670	650	647	610	560	558
3	4120	3940	3810	3790	3540	3390	3370
4	4250	4050	3910	3902	3680	3400	3470
5	4850	4700	4620	4601	4250	4140	4320
6	8660	8280	7990	7970	7550	6910	7270
7	10920	10480	10170	10160	9420	9080	9340
8	11390	10850	10480	10476	9870	9140	9350
9	14660	14220	13960	13923	12860	12520	13060
10	20140	19440	18940	18912	17450	16920	17540

Table 4 Natural frequencies for C-C MEE beam with different volume fractions

Mode No.	Natural Frequency (Hz)						
	$V_f = 0.0$	$V_f = 0.2$	$V_f = 0.4$	$V_f = 0.5$	$V_f = 0.6$	$V_f = 0.8$	$V_f = 1.0$
1	4160	3980	3850	3690	3570	3420	3419
2	4310	4100	3950	3910	3720	3440	3445
3	9730	94300	9260	8790	8530	8300	8660
4	10640	10240	9950	9440	9180	8870	9160
5	11200	10640	10260	10180	9660	8990	9200
6	17770	16930	16310	16300	15400	14110	14740
7	19410	18790	18350	17230	16850	16370	17050
8	19710	19110	18750	17800	17280	16730	17200
9	20730	19690	19010	18870	17880	16810	17540
10	30080	29250	28670	26710	26230	25610	26850

3.4 Static analysis

The structural behavior of the MEE beam subjected to various mechanical loading has been investigated. The MEE beam with clamped-clamped (CC) and clamped-free (CF) boundary conditions are considered for the analysis. In addition, analyzing the effects of boundary conditions and volume fractions on the direct quantities (displacements and potentials) of the MEE beam is also considered as the prime importance of this study.

3.4.1 Clamped-Clamped boundary condition

The behavior of the clamped-clamped MEE beam (U_x, U_v, U_w, ϕ, $\psi = 0$; at $x = 0$ and L) is investigated for two load cases. In the case-1, influence of uniformly distributed load (UDL) of q_0 = 5 kN/m acting over the beam length L is considered while case-2 refers to a point load of 5 kN acting at the midspan of the beam. For each loading case, the effect of different volume fractions (V_f) of the BaTiO$_3$ and CoFe$_2$O$_4$ (V_f = 0.0, 0.5 and 1.0) on the direct quantities are evaluated. V_f =
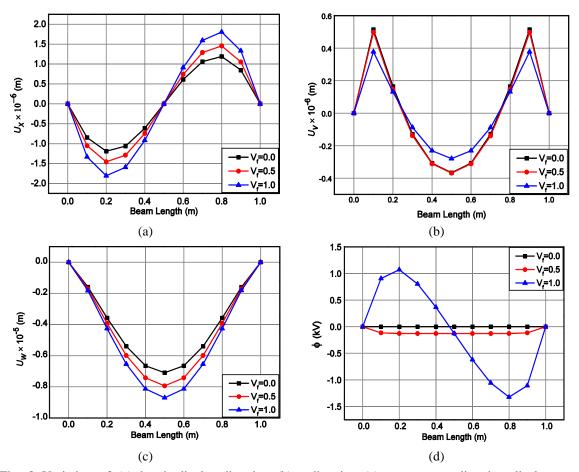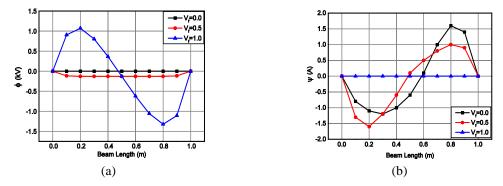
Fig. 3 Variation of (a) longitudinal *x*-direction (b) *y*-direction (c) transverse *z*-direction displacement components for CC-MEE beam subjected to UDL

0.0, 0.5 and 1.0 corresponds to the pure piezomagnetic (CoFe$_2$O$_4$), 50% BaTiO$_3$ and 50% CoFe$_2$O$_4$ and pure piezoelectric (BaTiO$_3$) phase, respectively.

   Case 1: Uniformly distributed load (UDL). The longitudinal *x*-direction displacement component (U_x), *y*-direction displacement component (U_v) and transverse *z*-direction displacement component (U_w) are plotted in Figs. 3(a)-(c), respectively. It may be observed from these figures that the maximum value of U_x and U_w is obtained for pure piezoelectric phase ($V_f = 1.0$) whereas, U_v is maximum for $V_f = 0.5$. At the mid span of the beam, it is witnessed that for all the volume fractions, the longitudinal *x*-direction displacement component U_x is zero while U_w is maximum. Further, the maximum value of U_v is observed at the region near the clamped end. From Fig. 4(a) it may be observed that the pure piezoelectric phase exhibits the maximum electric potential along the beam length. As it is expected that for the $V_f = 1.0$, the piezoelectric constants are higher in magnitude. Similarly, it may be seen from the Fig. 4(b) that the pure piezomagnetic phase $V_f = 0.0$ has a considerable effect on the magnetic potential of the MEE beam. The stress variation of the CC-MEE beam subjected to a uniformly distributed load (UDL) is illustrated in Figs. 5(a)-(e). Although from Fig. 5(a) it appears that the normal stress σ_x is independent on the volume fraction.

(a)   (b)

Variation of (a) electric potential (b) magnetic potential for the CC- MEE beam subjected to UDL
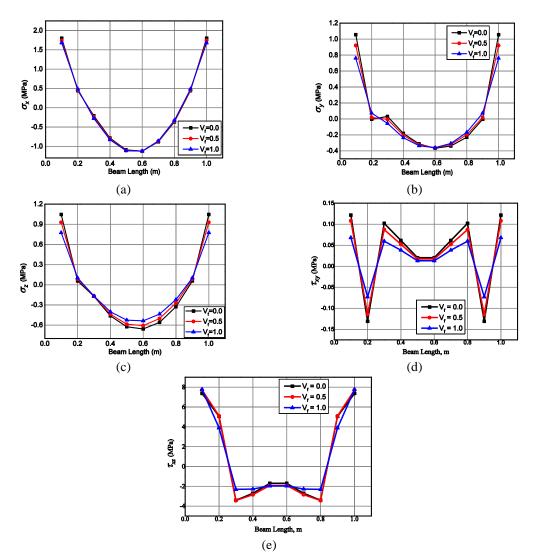

(a)   (b)

(c)   (d)

(e)

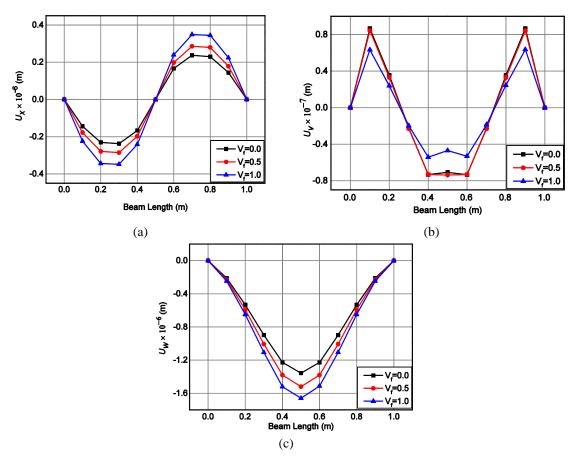Fig. 5 Variation of normal and shear stresses of the CC-MEE beam subjected to UDL (a) σ_x (b) σ_y (c) σ_z (d) τ_{xy} (e) τ_{xz}

(a)   (b)

(c)

Fig. 6 Variation of (a) U_x (b) U_v (c) U_w displacement components of CC- MEE beam subjected to a centre load

However, the careful observation reveals that the normal stress σ_x is maximum for $V_f = 0.0$. It may also be observed that the similar trend is followed by the stresses σ_y and σ_z. From Figs. 5(a)-(c), it may be noticed that the normal stresses follows a symmetrical distribution along the beam length. The shear stress τ_{xy} follows a zigzag pattern as shown in Fig. 5(d) whereas, τ_{xz} decreases initially upto a certain distance from the left clamp of the beam and then increases further as presented in Fig. 5(e).

Case 2: Central load. Figs. 6(a)-(c) illustrate the variation in the longitudinal x-direction, y-direction and transverse z-direction displacements components, respectively. It may be identified that all the displacement components follows a similar trend as that of the CC-MEE beam subjected to UDL as shown in Figs. 4(a)-(c). Figs. 7(a) and (b) illustrate the variation of ϕ and ψ of the C-C MEE beam subjected to central load. As seen from this figure at the midspan of the beam a sudden change in the electric potential is observed for $V_f = 0.5$. It may be attributed to the loading pattern considered. Fig. 7(b) illustrates that the magnetic potential follows the same trend as that of the CC-MEE beam with UDL as shown in Fig. 4(b). The normal stresses shown in Figs. (a)-(c) also follows the same trend as that of the CC-MEE beam with UDL. However, the fact that the graph is more confined towards the midspan of the beam. Further, the negligible influence
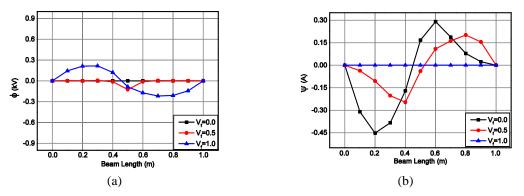
(a)

(b)

Fig. 7 Variation of the (a) electric potential (b) magnetic potential for the CC- MEE beam subjected to centre load
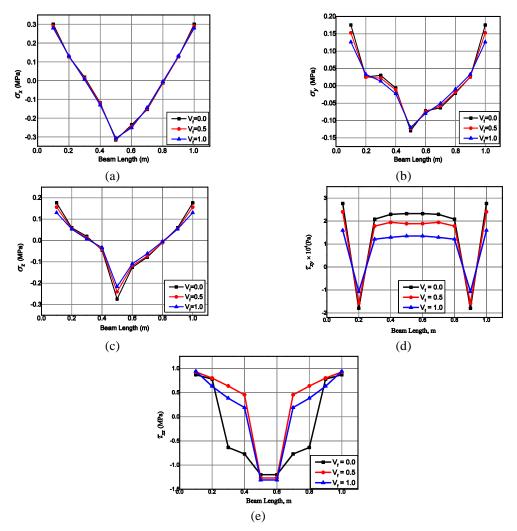

(a)

(b)

(c)

(d)

(e)

Fig. 8 Variation of normal and shear stresses of the CC-MEE beam subjected to centre load (a) σ_x (b) σ_y (c) σ_z (d) τ_{xy} (e) τ_{xz}
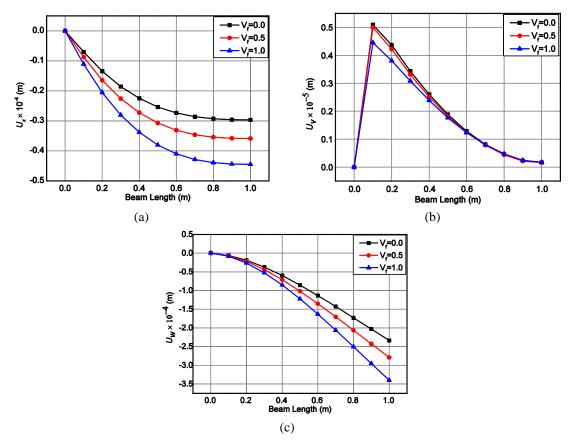
Fig. 9 Variation of (a) longitudinal *x*-direction (b) *y*-direction (c) transverse *z*-direction displacement components for CF- MEE beam subjected to UDL

of the volume fraction is observed for the normal stresses. Figs. 8(d) and (e) depict the shear stress variation of the CC-MEE beam.

3.4.2 Clamped-free condition

In this section, the cantilever MEE beam subjected to different loading cases such as uniformly distributed load and the end load is considered for the study. The variations of the direct quantities are investigated.

Case-1: Uniformly distributed load (UDL). A uniformly distributed load of $q_0 = 5$ kN/m is applied along the length of the CF- MEE beam. From Figs. 9(a)-(c), it may be observed that at the free end, the MEE beam experiences the maximum value of U_x and U_w. In the region near the clamped end, the U_v is maximum. For $V_f = 1.0$, maximum U_x and U_w is observed whereas, U_w is maximum for $V_f = 0.0$. Fig. 10(a) depicts the variation of the electric potential along the beam length. The maximum electric potential is observed near the clamped end for pure piezoelectric beam. Further from Fig. 10(b), it may be noticed that for $V_f = 0.5$, the CF-MEE beam displays the maximum magnetic potential. The normal stress distribution elucidated in Figs. 11 (a)-(c) suggest that the discrepancies with respect to the volume fractions can be clearly observed at the region near the clamped end where $V_f = 0.0$ has a predominant effect. It may be observed from Fig. 11(d)
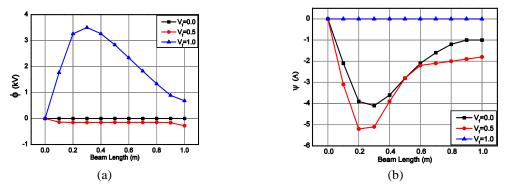
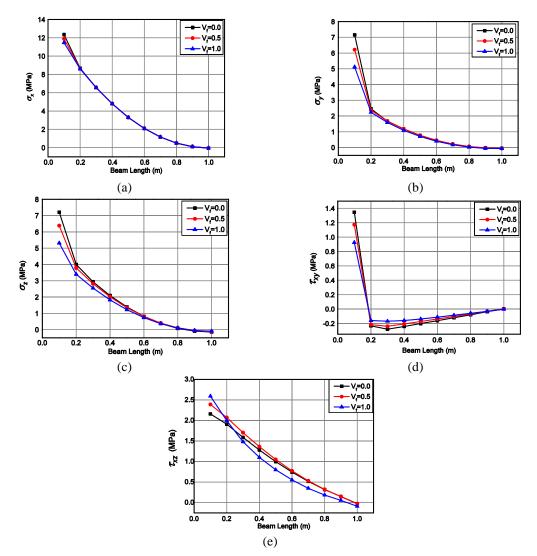Fig. 10 Variation of (a) electric potential (b) magnetic potential for the CF-MEE beam subjected to UDL

Fig. 11 Variation of normal and shear stresses of the CF-MEE beam subjected to UDL (a) σ_x (b) σ_y (c) σ_z (d) τ_{xy} (e) τ_{xz}
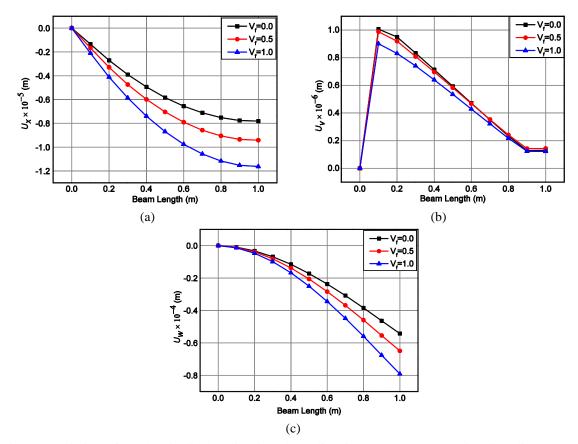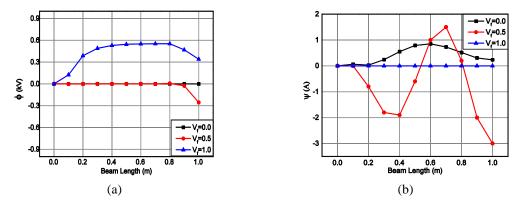
Fig. 12 Variation of (a) longitudinal *x*-direction (b) *y*-direction (c) transverse *z*-direction displacement components for CF- MEE beam subjected to end load

that starting at a distance from the clamped end, the shear stress τ_{xy} shows a linearly increasing trend along the beam length while Fig. 11(e) illustrates that the shear stress τ_{xz} gradually decreases along the beam length.

Case-2: End Load. In this case, the cantilever MEE beam is subjected to a point load of 5 kN at the free end. Figs. 12(a)-(c) elucidate the variation of the displacement components U_x, U_v, U_w, respectively. It is seen that these parameters follows the same trend as that of the CF-MEE beam with uniformly distributed load. From Fig. 13(a) it may be observed that for V_f=1.0, the electric potential rises to a certain value from the clamped end and remains almost constant over the beam length, which then decreases slightly at the free end. For V_f=0.5, a significant value of the electric potential is observed only at the free end. The electric potential values for V_f=0.5 is negligible as compared to V_f=1.0. The variation of the magnetic potential along the beam length is shown in Fig. 13(b). The maximum magnetic potential for V_f=0.0 is witnessed at the midspan of the beam whereas, for V_f=0.5 it is observed at the free end. The normal stresses for the CF-MEE beam with the end load are plotted in Figs. 14(a)-(c). Except at the region near the clamped end, a linear variation of these parameters along the beam length is observed. V_f= 0.0 displays the highest value of stresses. Similarly, from Fig. 14(d), it may be noticed that the shear stress τ_{xy} remain constant throughout the beam length whereas, Fig. 14(e) illustrates that the shear stress τ_{xz} varies linearly.

(a)　　　　　　　　　　　　　　　(b)

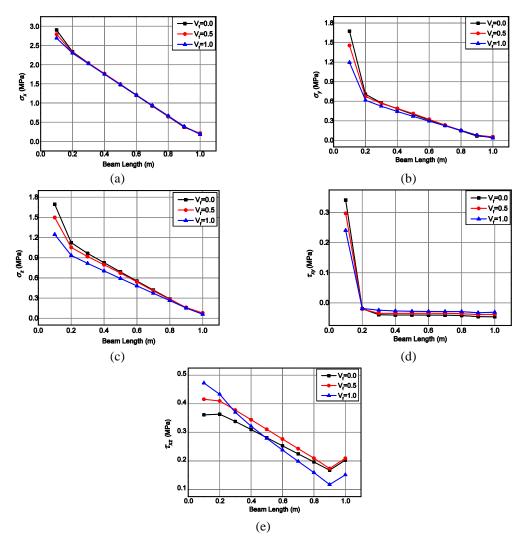Fig. 13 Variation of (a) electric potential (b) magnetic potential for the CF-MEE beam subjected to end load

(a)　　　　　　　　　　　　　　　(b)

(c)　　　　　　　　　　　　　　　(d)

(e)

Fig. 14 Variation of normal and shear stresses of the CF-MEE beam subjected to end load (a) σ_x (b) -σ_y (c) σ_z (d) τ_{xy} (e) τ_{xz}

4. Conclusions

In this work, a 3D finite element formulation has been presented to evaluate the natural frequency and static characteristics of MEE beam. The governing equations are formulated by minimization of total potential energy.

Adopting condensation technique, the nodal thermal displacements, electric potential and magnetic potential were computed. It is seen from the investigation that the volume fraction, boundary conditions have a significant effect on the free vibration and static characteristics of MEE beam. In particular, following conclusions can be made

1. The natural frequencies tend to increase with the increase in volume fraction of $BaTiO_3$ and $CoFe_2O_4$.

2. In contrast to point load, a significant effect of uniformly distributed loads on the electric and magnetic potentials of the system can be observed.

3. The maximum electric and magnetic potentials are observed at the region near the clamped end of the beam.

4. For the volume fraction $V_f = 0.0$, the MEE beam experiences highest normal stresses while the displacement components are minimum.

It is expected that this study may help in the design of the magneto-electro-elastic sensors and actuators in the real application.

References

Aktas, A. (2001), "Determination of the deflection function of a composite cantilever beam using theory of anisotropic elasticity", *Math. Comput. Appl.*, **6**(1), 67-74.

Annigeri, A.R., Ganesan, N. and Swarnamani, S. (2007), "Free vibration behaviour of multiphase and layered magneto-electro-elastic beam", *J. Sound Vibr.*, **299**(1-2), 44-63.

Arefi, M. and Zenkour, A.M. (2017), "Electro-magneto-elastic analysis of a three layer curved beam", *Smart Struct. Syst.*, **19**(6), 695-703.

Balu, S., Kannan, G.R. and Rajalingam, K. (2014), "Static studies on piezoelectric/piezomagnetic composite structure under mechanical and thermal loading", *IJERST*, **3**(2), 678-685.

Benedetti, I. and Milazzo, A. (2017), "Advanced models for smart multilayered plates based on reissner mixed variational theorem", *Compos. Part B: Eng.*, **119**, 215-229.

Bhangale, R.K. and Ganesan, N. (2006), "Free vibration of simply supported functionally graded and layered magneto-electro-elastic plates by finite element method", *J. Sound Vibr.*, **294**(4), 1016-1038.

Biju, B.N., Ganesan, N. and Shankar, K. (2011), "Dynamic response of multiphase magnetoelectroelastic sensors using 3D magnetic vector potential approach", *IEEE Sens. J.*, **11**(9), 2169-2176.

Carrera, E., Brischetto, S., Fagiano, C. and Nali, P. (2009), "Mixed multilayered plate elements for coupled magneto-electro-elastic analysis", *Multidiscipl. Model. Mater. Struct.*, **5**, 251-256.

Chen, J., Chen, H., Pan, E. and Heyliger, P.R. (2007), "Modal analysis of magneto-electro-elastic plates using the state-vector approach", *J. Sound Vibr.*, **304**, 722-734.

Ebrahimi, F. and Barati, M.R. (2016a), "A nonlocal higher-order magneto electro visco-elastic beam model for dynamic analysis of smart nanostructures", *J. Eng. Sci.*, **107**, 183-196.

Ebrahimi, F. and Barati, M.R. (2016b), "Dynamic modeling of a thermos-piezo-electrically actuated nanosize beam subjected to a magnetic field", *Appl. Phys. A*, **122**(4), 451.

Ebrahimi, F. and Barati, M.R. (2016c), "Magnetic field effects on dynamic behavior of inhomogeneous thermo-piezo-electrically actuated nanoplates", *J. Brazil. Soc. Mech. Sci. Eng.*, **39**(6), 2203-2223.

Ebrahimi, F., Jafari, A. and Barati, M.R. (2017), "Vibration analysis of magneto-electro-elastic

heterogeneous porous material plates resting on elastic foundations", *Thin-Wall. Struct.*, **119**, 33-46.

Fan, X. and Wu, Z. (2016), "C$_0$-type Reddy's theory for composite beams using FEM under thermal loads", *Struct. Eng. Mech.*, **57**(3), 457-471.

Huang, D.J., Ding, H.J. and Chen, W.Q. (2007), "Analytical solution for functionally graded magneto-electro-elastic plane beams", *J. Eng. Sci.*, **45**, 467-485.

Jandaghian, A.A. and Rahmani, O. (2016), "Free vibration analysis of magneto-electro-thermo-elastic nanobeams resting on a Pasternak foundation", *Smart Mater. Struct.*, **25**(3), 035023.

Kattimani, S.C. (2017), "Geometrically nonlinear vibration analysis of multiferroic composite plates and shells", *Compos. Struct.*, **163**, 185-194.

Kattimani, S.C. and Ray, M.C (2014a), "Smart damping of geometrically nonlinear vibrations of magneto-electro-elastic plates", *Compos. Struct.*, **114**(1), 51-63.

Kattimani, S.C. and Ray, M.C. (2014b), "Active control of large amplitude vibrations of smart magneto-electro-elastic doubly curved shells", *J. Mech. Mater. Des.*, **10**(4), 351-378.

Kattimani, S.C. and Ray, M.C. (2015), "Control of geometrically nonlinear vibrations of functionally graded magneto-electro-elastic plates", *J. Mech. Sci.*, **99**, 154-167.

Kondaiah, P., Shankar, K. and Ganesan, N. (2015), "Pyroeffects on magneto-electro-elastic sensor bonded on mild steel cylindrical shell", *Smart Struct. Syst.*, **16**(3), 537-554.

Kondaiah, P., Shankar, K. and Ganesan, N. (2017), "Pyroeffects on magneto-electro-elastic sensor patch subjected to thermal load", *Smart Struct. Syst.*, **19**(3), 299-307.

Kondaiah. P., Shankar, K. and Ganesan, N. (2012), "Studies on magneto-electro-elastic cantilever beam under thermal environment", *Coupled Syst. Mech.*, **1**(2), 205-217.

Lage, R.G. and Soares, C.M.M. (2004), "Layerwise partial mixed finite element analysis of magneto-electro-elastic plates", *Comput. Struct.*, **82**, 1293-1301.

Milazzo, A. (2013), "A one-dimensional model for dynamic analysis of generally layered magneto-electro-elastic beams", *J. Sound Vibr.*, **332**(2), 465-483.

Milazzo, A., Orlando, C. and Alaimo, A. (2009), "An analytical solution for the magneto-electro-elastic bimorph beam forced vibrations problem", *Smart Mater. Struct.*, **18**(8), 85012.

Pan, E. and Han, F. (2005), "Exact solution for functionally graded and layered magneto-electro-elastic plates", *J. Eng. Sci.*, **43**(3-4), 321-339.

Simoes Moita, J.M., Mota Soares, C.M. and Mota Soares, C.A. (2009), "Analyses of magneto-electro-elastic plates using a higher order finite element model", *Compos. Struct.*, **91**(4), 421-426.

Simsek, M. and Reddy, J.N. (2013), "Bending and vibration of functionally graded microbeams using a new higher order beam theory and the modified couple stress theory", *J. Eng. Sci.*, **64**, 37-53.

Sladek, J., Sladek, V., Krahulec, S. and Pan, E. (2013), "The MLPG analyses of large deflections of magnetoelectroelastic plates", *Eng. Analy. Bound. Elem.*, **37**(4), 673-682.

Sladek, J., Sladek, V., Repka, M., Kasala, J. and Bishay, P. (2017), "Evaluation of effective material properties in magneto-electro-elastic composite materials", *Compos. Struct.*, **174**, 176-186.

Vaezi, M., Shirbani, M.M. and Hajnayeb, A. (2016), "Free vibration analysis of magneto-electro-elastic microbeams subjected to magneto-electric loads", *Phys. E: Low-Dimens. Syst. Nanostruct.*, **75**, 280-286.

Vinyas, M. and Kattimani, S.C. (2017c), "Static behavior of thermally loaded multilayered magneto-electro-elastic beam", *Struct. Eng. Mech.*, **63**(4), 481-495.

Vinyas, M. and Kattimani, S.C. (2017e), "Multiphysics response of magneto-electro-elastic beams in thermo-mechanical environment", *Coupled Syst. Mech.*, **3**(4), 351-367.

Vinyas, M. and Kattimani, S.C. (2017f), "Hygrothermal analysis of magneto-electro-elastic plate using 3D finite element analysis", *Compos. Struct.*, **180**, 617-637.

Vinyas, M. and Kattimani, S.C. (2017a), "Static studies of stepped functionally graded magneto-electro-elastic beam subjected to different thermal loads", *Compos. Struct.*, **163**, 216-237.

Vinyas, M. and Kattimani, S.C. (2017b), "Static analysis of stepped functionally graded magneto-electro-elastic plates in thermal environment: A finite element study", *Compos. Struct.*, **178**, 63-86.

Vinyas, M. and Kattimani, S.C. (2017d), "A Finite element based assessment of static behavior of multiphase magneto-electro-elastic beams under different thermal loading", *Struct. Eng. Mech.*, **62**(5),

519-535.

CC

Appendix A

σ_i	Stress tensor
Ω	Volume
η_{lk}	Dielectric constant matrix
μ_{lk}	Magnetic permeability constant matrix
ε_j	Linear strain tensor
ρ	Density
B_l	Magnetic induction vector
C_{ij}	Elastic stiffness matrix
D_l	Electric displacement vector
E_k	Electric field vector
e_{lj}	Piezoelectric co-efficient matrix
H_k	Magnetic co-efficient vector
m_{lk}	Electromagnetic co-efficient matrix
Q^ϕ	Electric charge density
Q^ψ	Magnetic current density
q_{lj}	Magnetostrictive co-efficient matrix
$\{F_{surface}\}$	Surface load vector
$\{F_{body}\}$	Body force vector
$\{F_{conc}\}$	Concentrated load vector
$[K_{uu}^e]$	Elemental elastic stiffness matrix
$[K_{u\phi}^e]$	Elemental electro-elastic coupling stiffness matrix
$[K_{u\psi}^e]$	Elemental magneto-elastic coupling stiffness matrix

$[K_{\phi\phi}^e]$ Elemental electric stiffness matrix

$[K_{\psi\psi}^e]$ Elemental magnetic stiffness matrix

$[K_{\phi\psi}^e]$ Elemental electro-magnetic stiffness matrix

$[M^e]$ Elemental mass matrix

Appendix B

$$\left[K_{uu}^{e}\right]=\int_{\Omega}\left[B_{u}\right]^{T}\left[C\right]\left[B_{u}\right]d\Omega,\ \left[K_{u\phi}^{e}\right]=\int_{\Omega}\left[B_{u}\right]^{T}\left[e\right]\left[B_{\phi}\right]d\Omega,\ \left[K_{u\psi}^{e}\right]=\int_{\Omega}\left[B_{u}\right]^{T}\left[q\right]\left[B_{\psi}\right]d\Omega,$$

$$\left[K_{\phi\phi}^{e}\right]=\int_{\Omega}\left[B_{\phi}\right]^{T}\left[\eta\right]\left[B_{\phi}\right]d\Omega,\ \left[K_{\phi\psi}^{e}\right]=\int_{\Omega}\left[B_{\phi}\right]^{T}\left[m\right]\left[B_{\psi}\right]d\Omega,\ \left[K_{\psi\psi}^{e}\right]=\int_{\Omega}\left[B_{\psi}\right]^{T}\left[\mu\right]\left[B_{\psi}\right]d\Omega \quad \text{(B1)}$$

$$\left[M^{e}\right]=\rho\int_{\Omega}\left[N\right]^{T}\left[N\right]d\Omega$$

The different shape function derivative matrices appearing in Eq. (B1) are given by

$$\left[B_{u}\right]=\begin{bmatrix} \dfrac{\partial N_{i}}{\partial x} & 0 & 0 \\[6pt] 0 & \dfrac{\partial N_{i}}{\partial y} & 0 \\[6pt] 0 & 0 & \dfrac{\partial N_{i}}{\partial z} \\[6pt] 0 & \dfrac{\partial N_{i}}{\partial z} & \dfrac{\partial N_{i}}{\partial y} \\[6pt] \dfrac{\partial N_{i}}{\partial z} & 0 & \dfrac{\partial N_{i}}{\partial x} \\[6pt] \dfrac{\partial N_{i}}{\partial y} & \dfrac{\partial N_{i}}{\partial x} & 0 \end{bmatrix}, \quad \left[B_{\psi}\right]=\begin{bmatrix} \dfrac{-\partial N_{i}}{\partial x} \\[6pt] -\dfrac{\partial N_{i}}{\partial y} \\[6pt] -\dfrac{\partial N_{i}}{\partial z} \end{bmatrix}, \quad \left[B_{\phi}\right]=\begin{bmatrix} \dfrac{-\partial N_{i}}{\partial x} \\[6pt] -\dfrac{\partial N_{i}}{\partial y} \\[6pt] -\dfrac{\partial N_{i}}{\partial z} \end{bmatrix} \quad \text{(B2)}$$

where, $i=1, 2, 3, \ldots, 8$ represents the node numbers